Seismological aspects of the Cairo earthquake, 12th October 1992

Kamal M. Abou Elenean ([1]), **Hesham M. Hussein** ([1]), **Ahmad S. Abu El-Ata** ([2]) **and Ezzeldien M. Ibrahim** ([1])
([1]) *National Research Institute of Astronomy and Geophysics, Helwan, Cairo, Egypt*
([2]) *Faculty of Science, Ain Shams University, Cairo, Egypt*

Abstract
On 12 October 1992 a significant earthquake (M_B = 5.8) occurred southwest of Cairo in the vicinity of the Dahshour region. For the mainshock, an average moment release M_0 = 9.70E17 n-m; a fault length = 13.8 km; an average displacement = 0.22 m; a stress drop = 0.760 MPa and maximum spectral magnitude = 5.78 were obtained. Spectral magnitude calculations were used in this analysis. The distribution of the well-recorded aftershocks over 15 months using a temporary seismic network installed immediately after the mainshock shows a zone of concentrated activity. Three composite focal mechanism solutions are constructed, using *P* wave polarity data for 30 earthquakes. These solutions have a mechanism, involving normal and right lateral strike slip motion along E-W to ENE-WSW trending fault plane. The *P*-wave polarity data of the individual 30 earthquakes are inverted to determine the stress tensor. The stress field estimated is extensional with σ_3 in the direction of NNE. The stress pattern determined from the inversion is in good agreement with the one estimated from the three composite fault plane solutions, while the neotectonic situation in Northern Egypt supports ENE-WSW extensional movement. However, the region of study has suffered both extensional tectonic activity of the Northern Red Sea rift zone and the compressional tectonic activity along the Hellenic arc. The inconsistency of the principal tension directions may belong to the interaction between the extensional and compressioal tectonics.

Key words *Cairo earthquake – source parameters – spectral magnitude – focal mechanism – aftershock – stress tensor inversion*

1. Introduction

On Monday, 12th October 1992 at 15:09 local time, a damaging earthquake of magnitude M_W = 5.8 took place in Dahshour region, about 25 km SW of downtown Cairo at the coordinates 29.77N, 31.07E (fig. 1) and was followed by a sequence of aftershocks. According to the instrumental data, the focal depth of this event was 23 km. The earthquake area had been considered as a region of relatively low seismic activity. In this century, the only other earthquake known to have occurred in this region is the 4.9 M_S event of October 1,1920 at 29.5°N , 31.3°. The only known earthquake during the historical period occurred in August 1847 A.D. and destroyed 3000 houses and 42 mosques in Cairo and Northern Egypt (Kebeasy *et al.*, 1981). The Cairo earthquake was also the first earthquake in this region to be recorded teleseismically by the Worldwide Standard Seismograph Network and the Global Digital Seismograph Network. The recent Cairo earthquake was felt in much of Egypt from Alexandria to Aswan. Significant losses of life and property were reported in the Faiyum basin, the Nile Delta and

Mailing address: Dr. Hesham Hussein Mohamed Moussa, P.O. Box 70, Helwan 11421, Cairo, Egypt; e-mail: hesham65 @hotmail.com

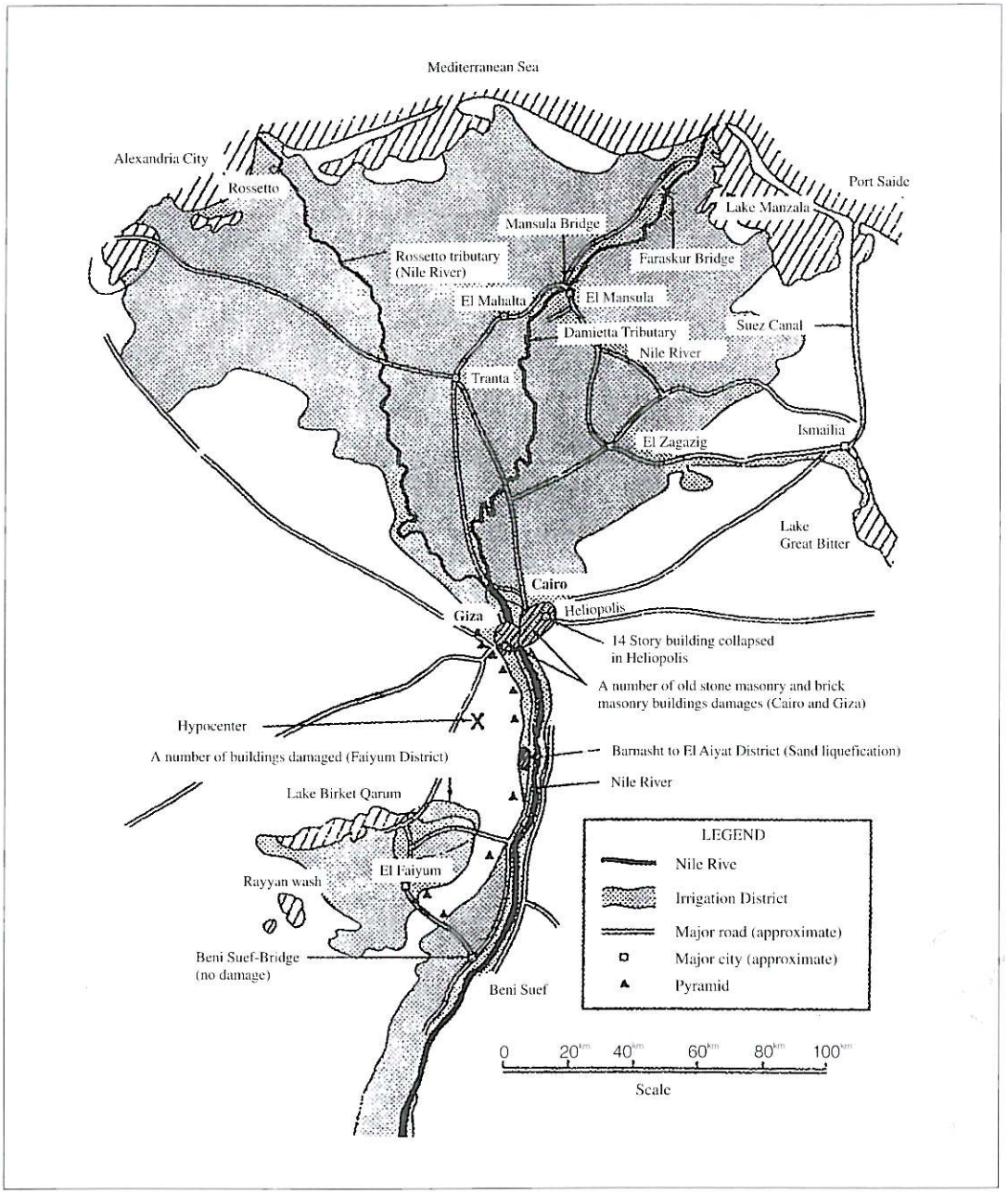

Fig. 1. Locations of the sand liquefaction and areas seriously damaged (Japanese Expert Team, 1993).

along the Nile River (fig. 1). At least 561 people were killed, about 12 192 injures were reported, more than 20 000 people became homeless and 8300 buildings were damaged or destroyed in the Cairo area alone. The economic losses of this earthquake reached 4 billion US dollars.

The Japanese Expert Team (1993) evaluated the damage caused by this earthquake (fig. 1). Devastating damage was reported in downtown Cairo but most damage was confined to old masonry structures, including churches, Islamic historical buildings and mosques. Minor damage such as cracks on walls and falling plaster typify the damage incurred by modern buildings in downtown Cairo, the collapse of a 14 story building in the Heliopolis being the primary exception. Based upon this damage the seismic intensity in downtown Cairo is estimated as VI in MSK scale. Adobe structures in suburban area such as El Faiyum and Al Aiyat were seriously damaged (VII). Temporary housing camps were set up at some villages of Al Aiyat and El Faiyum. The maximum macroseismic intensity was evaluated I_0 = VII-VIII in the epicentral region. On the basis of macroseismic intensity survey conducted by the National Research Institute of Astronomy and Geophysics (NARIAG-Egypt) the highest seismic intensity was observed in the regions of unconsolidated sediments in the Nile Delta, the Faiyum basin and along the Nile River.

Liquefaction was also observed at Barnasht and El Aiyat along the Nile (fig. 1), 19 km from the focus (Japanese Expert Team, 1993). In Barnasht, six large sand valves, 3 to 4 m in diameter were found in crop field. Holes were 1 and 2 m deep and the surface was covered with clay soil deposits 1 m thick, with a mean strike elongation N 70° to N 110°. Underneath the clayey soil deposits, sand deposits were found. According to eyewitnesses, sand and water continuously blew up to a height of 3 m for about 45 min. In the epicentral region, the National Research Institute of Astronomy and Geophysics (NRIAG) and the Egyptian Geological Survey (EGS) teams observed segments of fresh ground cracks trending NW-SE, E-W and N 10°E. These cracks show no systematic displacement. West of Dahshour region, a fresh open fracture strikes in an E-W direction and has a visible length of about 1200 m (Abd El-Tawb *et al.*, 1993). The field observations also include subsidence of the left-hand side of the asphalt road between Aiyat and Giza. Maximum subsidence was about 1.5 m.

The purpose of this work is the study of the Cairo earthquake and its sequence, based on the distribution of aftershocks, the determined mechanisms, the tectonic setting and the dynamic source parameters of the mainshock. In this study, focal mechanism solutions have been derived for some aftershocks. Polarities were obtained from an analysis of the data from the instrumental field survey conducted by NRIAG. The 12th October 1992 earthquake and its sequence are the first in this region for which fault plane solutions are derived. Investigation of these mechanisms is the only clue to the new tectonic situation in this region. In addition to determination of the fault planes, P and T axes are also obtained. These results may shed light on the local stress field of this relatively low seismicity region. An attempt was also made to determine the mean principle stresses of this area from earthquake focal mechanism data, using computer based inversion processes. The method used here has been described in details by Gephart and Forsyth (1984). The source parameters (seismic moment, fault length, and stress drop) have been computed on the basis of spectral magnitude calculations.

2. Tectonic setting

The earthquake area is situated in the northern part of the western desert tectonic zone, which forms part of the African plate. Independent data from geophysical studies in this zone detected the presence of faults trending E-W or Tethyan trend (most significant), NE-SW, and NW-SW (Refai *et al.*, 1973; Meshref, 1990). Interpretation of the available seismic profiles and bore hole observations in this zone reflected the existence of two main systems of normal faulting (Sehim *et al.*, 1992). The first trends WNW to E-W while the second trends NW-SE. The WNW to E-W faults are of diagonal slip movements where the horizontal sense of dislocation is always of right-lateral type, while the

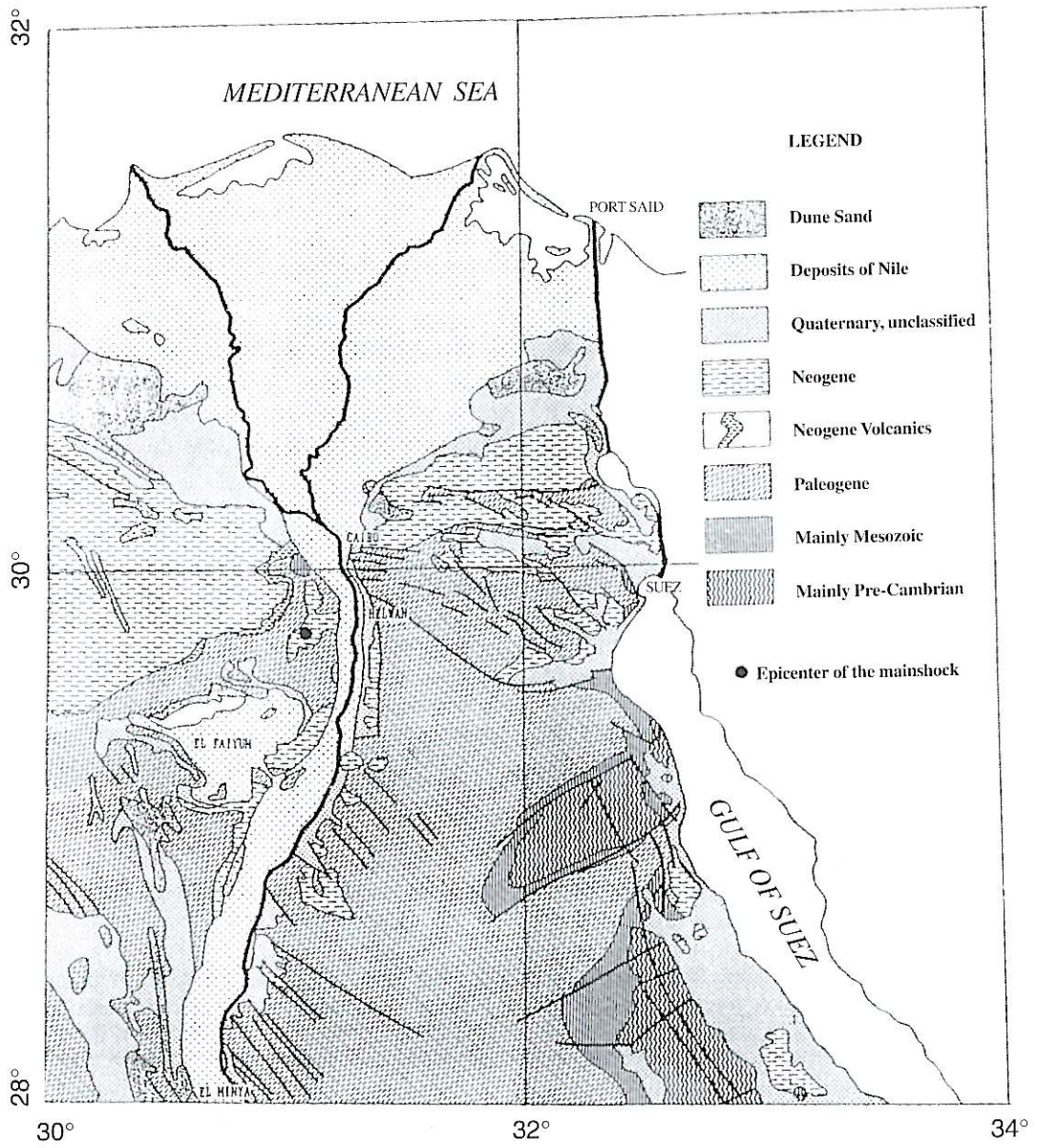

Fig. 2. Geological map of the Northern Egypt simplified from Egyptian Geological Survey (1981).

vertical displacements are of normal sense. The NW striking faults are of normal type.

The structural pattern in the northwestern zone reflects the dextral transcurrent motion between Africa and Laurasia during the Late Cretaceous to Paleocene time (Roberston Research International, 1982). This transcurrent motion was partially accompanied or partially followed by N-S or NNW-SSE horizontal compressional force upon Northeastern Africa in-

cluding Egypt. The continuation of this force resulted in rifting of the Red Sea and Gulf of Suez at a later time, most probably Oligocene. The direction of the regional horizontal extension becomes ENE-WSW. Therefore, Northern Egypt including the zone of the northwestern desert may be regarded as having been under a regional ENE-WSW extension from mid Tertiary to the present time (Meshref, 1990).

In the earthquake area, three main lithological categories can be distinguished (fig. 2): 1) unconsolidated Quaternary sediments in Faiyum basin, the Nile Delta and along the Nile River (Nile deposits); 2) limestone and clastic sediments of Paleogene, and 3) Neogene formations which consist mainly of clastic sediments of Miocene age, covering most of the northen part of the western desert.

3. Aftershock distribution

Immediately after the mainshock, the National Research Institute of Astronomy and Geophysics deployed a temporary seismic network of eight analog short period Sprengnether MEQ-800 portable seismographs to monitor the aftershock activity. Installation of the first station began on October 13, 24 h after the mainshock. During nearly one week, field seismographs were operated at 9 sites. Stations WEL, ASK and MRQ were closed on October, 18, October, 22 and November, 1 respectively. On November, 3 two additional stations were sited at new locations (DER and DHP). Time corrections for the portable recorders were made daily, using Russian time-signal transmission. Figure 3a illustrates the distribution of the temporary stations occupied during the aftershock study. Table I gives the station coordinates and dates when the stations were operated and closed. These stations plus three permanent short period stations at Helwan, Kottamia and El Mina (fig. 4) were used for locating the aftershocks. For accurate hypocenter determination, we measured *P* and *S* arrival times for all earthquakes that were recorded at most of the stations ($M_L > 1.9$) and the HYPO71 program (Lee and Lahr, 1972) was used to locate the aftershocks. It has been pointed out by a number of authors that the use of accurate *S* wave arrival times greatly improves the location accuracy, especially hypocentral depth (Soufleris *et al.*, 1982). Since our array is mainly analog vertical component instruments, picking the *S*-wave arrival times is usually difficult. Therefore, only inplusive *S* wave arrivals were used in the location process. Two crustal models D1 and D2 (table II) were tested by use in HYPO71 to locate the aftershocks. The D1 model yielded the smallest ERH, ERZ and rms residuals. The crustal model D1 consists of three layers overlying a half space (EL Hadidy, 1995), assuming a V_p/V_s ratio of 1.73. During the study period a large number of earthquakes were recorded. Earthquakes with a precision of better than 2.3 km in both horizontal plane and focal depth was selected and are shown in fig. 3a. All these events were located using at least six *P*-wave and two *S* arrivals. The maximum rms residual is 0.28 and the maximum azimuth gap between recording stations is equal to 150°. The pattern of aftershocks reveals an irregular spatial distribution, expressed as a cluster of seismicity. The same pattern was obtained by Maamoun *et al.* (1993). Figure 3a also shows that most of the aftershocks took place south of the mainshock. Figure 3b is a vertical profile oriented along line A-A$^-$ in fig. 3a. This profile A-A$^-$ is perpendicular to the fault plane of the mainshock. The distribution of the hypocenters does not delineate a clear fault plane. This phenomenon has been observed in other well-studied recent earthquakes (Deschamps and King, 1984). This may support the assumption that there is no simple relation between planes that moved in the mainshock and planes that moved to create aftershocks.

4. Focal mechanisms of the aftershocks

P wave polarity data for 30 earthquake which occurred in the area of Dahshour were used to construct three composite solutions (A, B and C), using the software package for the focal mechanism solution (Suetsugu, 1995). The initial study of the vertical cross section plot A-A$^-$ (fig. 5a,b) for the 30 aftershocks led us to divide them into three groups (A, B and C). Grouping of the 30 events provides a good basis for

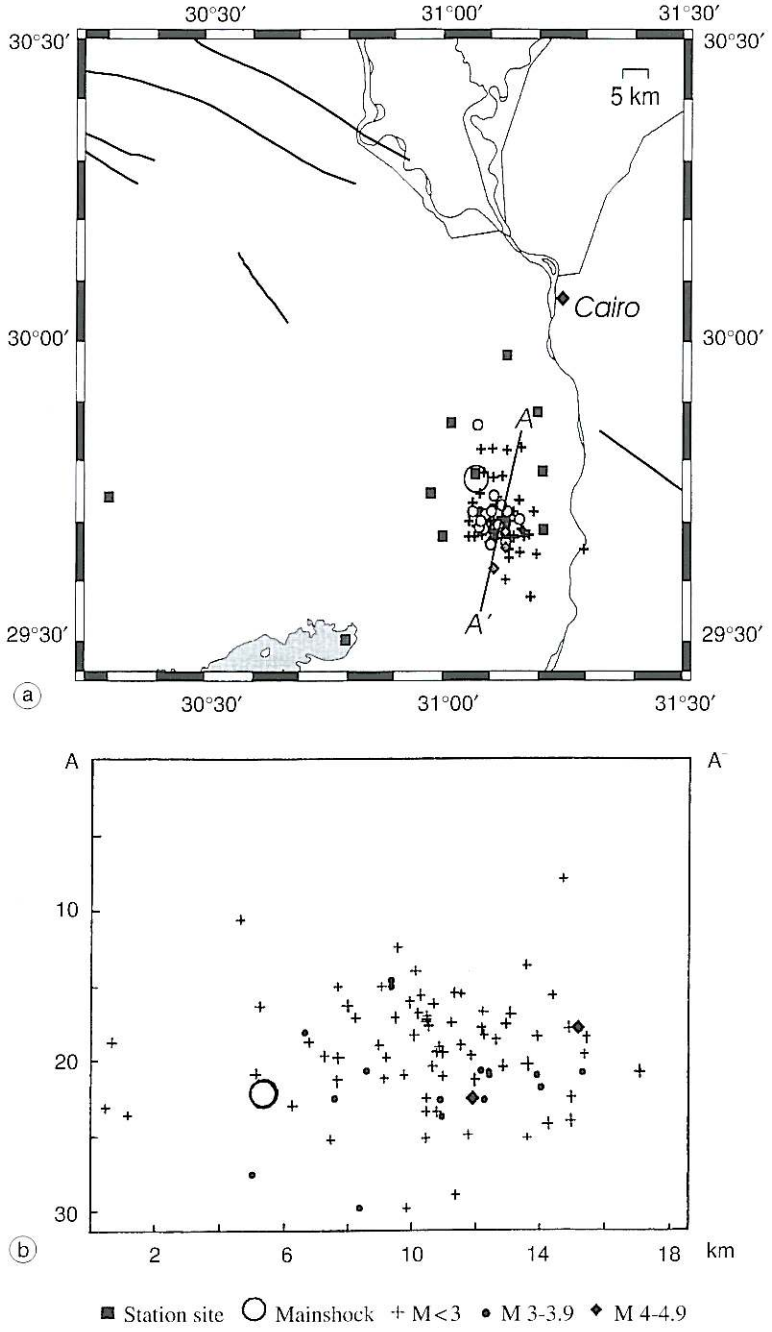

Fig. 3a,b. Epicentral distribution of the relocated aftershocks with error smaller than 2.3 km in focal depth and horizontal axis (a) and vertical section plot A-A¯ for the aftershocks (b).

Table I. Station coordinates.

Seismic station		Coordinates		Date of operation	Closed date
Name	Code	Lat.°N	Long.°E		
Sakkara	SAK	29.850	31.20	October 13, 1992	December 31, 1993
El-Ayat	AUT	29.666	31.18	October 14, 1992	December 31, 1993
Dahshour	DUS	29.773	31.07	October 15, 1992	December 31, 1993
Kom Oshem	ASK	29.503	30.707	October 15, 1992	October 22, 1992
Wl-Mayadeen	MDN	29.844	31.00	October 16, 1992	December 31, 1993
El- Beir	WEL	29.674	30.932	October 18, 1992	October 19, 1992
El Fayum	FUM	29.671	31.014	October 18, 1992	December 31, 1993
El-Morakaba	MRQ	29.748	30.301	October 21, 1992	November 1, 1992
El-Dair	DER	29.690	30.975	November 3, 1992	December 31, 1993
Haram Dahshour	DHP	29.783	31.210	November 3, 1992	December 31, 1993

Table II. Velocity models for Northern Egypt.

Model	Layer	Thickness (km)	V_p (km/s)	Reference
D1	1	3	4.5	El Hadidy (1995)
	2	13	6.0	
	3	15	6.5	
D2	1	3.5	3.5	Marzouk (1987)
	2	18.5	6.0	
	3	11.0	6.35	

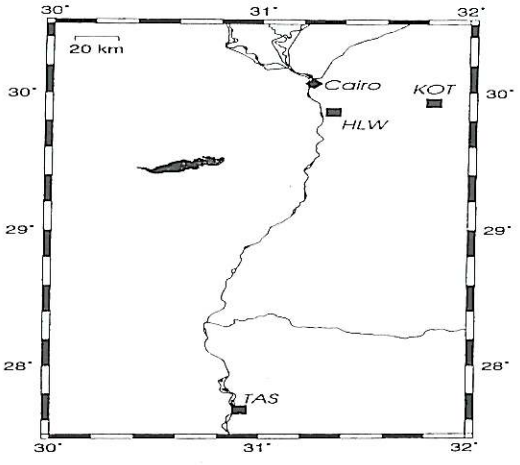

Fig. 4. Locations of the permanent stations.

driving the three composite solutions. The events for each group were checked for location proximity and uniformity of polarity pattern as is possible before constructing the composite fault plane solution. Table III shows the data used to construct these solutions. The fault plane parameters of these solutions are shown in table IV. These data were read by the authors from the seismograms recorded by the temporary network installed by NRIAG. The constructed solutions are presented in fig. 6. The lower hemisphere projection of the individual fault plane solutions for the 30 earthquakes is also shown in fig. 7. The data used and the parameters obtained are also shown in tables III and V.

For the three composite solutions, motion on the fault planes is predominantly dip slip with a right lateral strike slip motion on E-W trending fault plane for group A and ENE-WSW trending fault plane for groups B and C. We preferred the E-W to ENE-WSW striking plane because the geological evidence indicates dominating E-W right lateral strike faults in this area. High dip angles faulting in excess of 52° were obtained for the three groups. The composite mechanisms associated with the aftershocks of groups A and B are nearly consistent. The composite solution of group C seems to be similar to that of the other two groups except that the chosen fault plane has changed from dipping NNE (groups A and B) to dipping SSW (group C). In

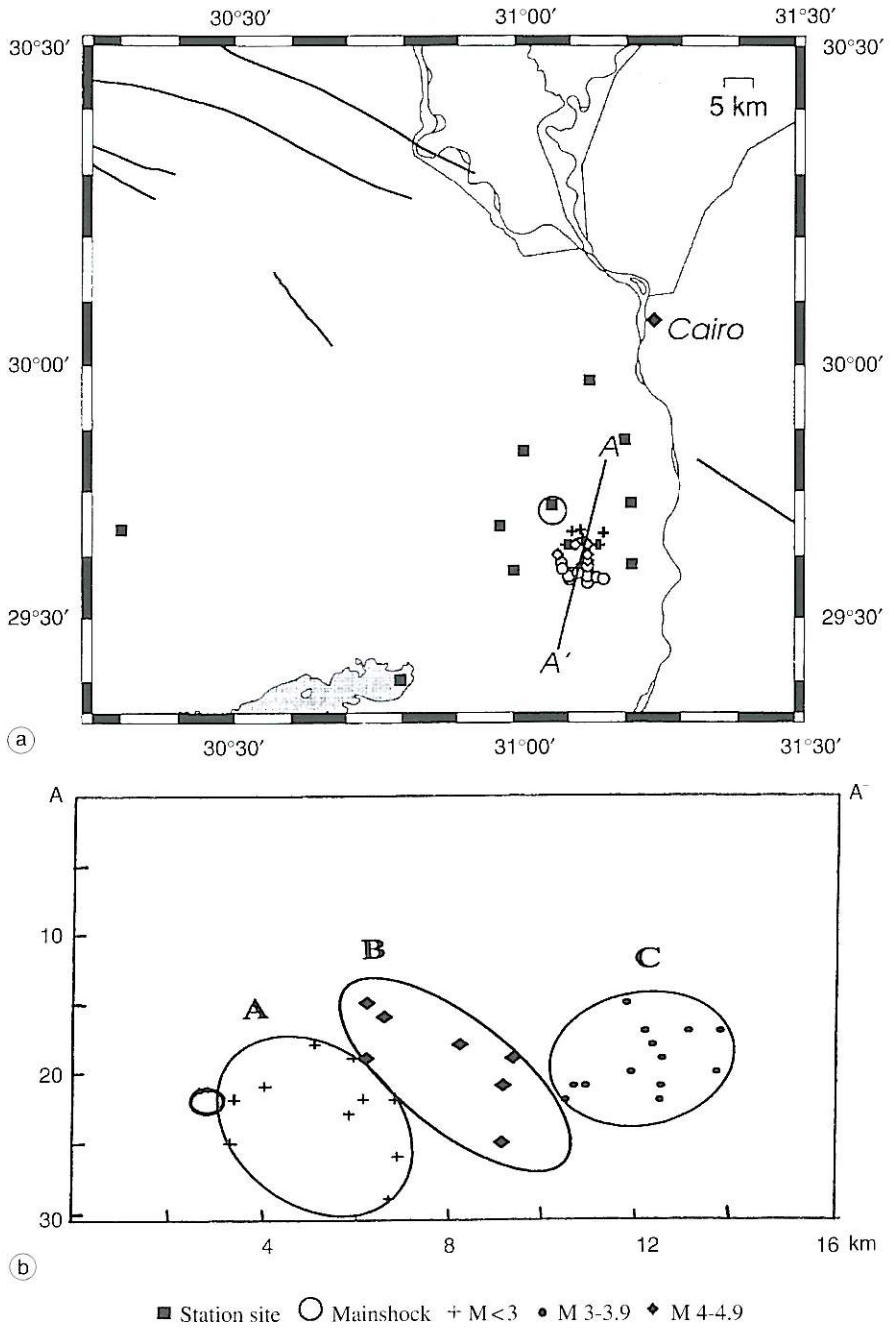

Fig. 5a,b. Epicentral distribution (a) and vertical section plot A-A⁻ (b) for the 30 aftershocks used in composite fault plane solutions.

Table III. List of earthquake events used in the construction of composite fault plane solutions for Dahshour region.

Event No.	Date			Origin time			Location		Depth	M_D(HLW)	Group
	D	M	Y	h	min	s	Lat.	Long.	H (km)		
1	18	10	1992	08	12	15.68	29.662	31.161	19	2.9	B
2	19	10	1992	12	30	16.62	29.653	31.133	21.5	3.2	A
3	19	10	1992	14	59	49.30	29.716	31.097	22	3.0	A
4	22	10	1992	08	28	59.18	29.678	31.088	15	3.2	B
5	25	10	1992	09	05	05.46	29.716	31.149	19.7	2.7	A
6	25	10	1992	12	26	16.02	29.681	31.114	17.5	2.8	B
7	25	10	1992	19	45	35.24	29.716	31.136	22.5	3.1	A
8	26	10	1992	06	45	23.34	29.716	31.103	29.89	3.1	A
9	30	10	1992	14	08	11.66	29.716	31.094	26	2.7	A
10	31	10	1992	01	43	11.50	29.716	31.154	23	2.7	A
11	04	11	1992	16	29	38.90	29.716	31.133	19.62	3.5	C
12	05	11	1992	18	41	50.51	29.682	31.133	22.5	4.2	B
13	05	11	1992	18	46	04.84	29.661	31.101	20.88	3.6	B
14	05	11	1992	19	16	47.33	29.671	31.133	20.74	3.9	B
15	06	11	1992	02	42	02.98	29.700	31.133	18	3.7	C
16	06	11	1992	04	11	16.60	29.671	31.107	18	2.8	B
17	07	11	1992	01	35	03.14	29.666	31.133	21	3.5	B
18	10	11	1992	11	17	18.78	29.656	31.133	17.8	4.0	B
19	10	11	1992	13	35	28.18	29.716	31.133	15	2.9	C
20	23	11	1992	22	58	07.95	29.735	31.161	25.78	2.7	A
21	02	12	1992	20	43	06.31	29.691	31.133	19.45	2.5	C
22	03	12	1992	06	38	10.43	29.699	31.111	16.68	2.3	C
23	22	01	1993	20	27	08.11	29.664	31.149	22.79	2.8	B
24	23	01	1993	00	04	48.38	29.700	31.080	25.27	2.8	C
25	17	02	1993	19	03	05.83	29.700	31.079	21.12	2.9	C
26	10	03	1993	19	26	52.30	29.726	31.124	18.16	3.8	A
27	04	05	1993	20	56	51.04	29.680	31.123	21	3.7	B
28	13	05	1993	08	38	25.62	29.687	31.086	21.7	3.1	B
29	13	06	1993	06	16	08.64	29.671	31.116	17.6	3.9	B
30	22	08	1993	17	58	06.51	29.740	31.115	22.36	2.3	A

Table IV. Table of fault plane parameters for the three composite solutions.

Event No.	Plane (1)			Plane (2)			P-axis		T-axis	
	Az.	Dip	Slip	Az.	Dip	Slip	Az.	Pl.	Az.	Pl.
A	161	58	−40	275	52	−145	122	48	217	04
B	164	57	−08	259	82	−150	127	30	27	17
C	75	56	−120	304	46	−50	288	62	188	05

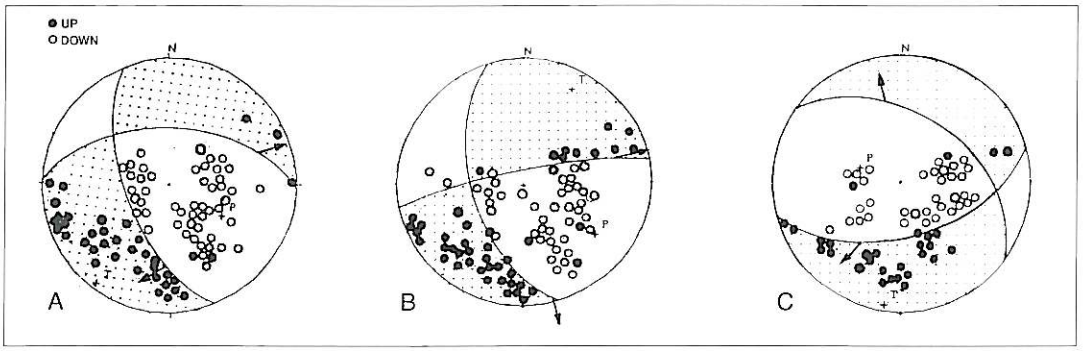

Fig. 6. The three composite solutions for the Cairo earthquake aftershocks.

Table V. Fault plane parameters of the individual events.

Event No.	Date			O. T.		Plane (1)		Plane (2)		*P*-axis		*T*-axis	
	D	M	Y	h	min	Az.	Dip	Az.	Dip	Az.	Pl.	Az.	Pl.
1	18	10	1992	08	12	106	44	292	46	275	87	19	01
2	19	10	1992	12	30	142	63	261	46	101	54	205	10
3	19	10	1992	14	59	140	52	265	53	113	59	23	00
4	22	10	1992	08	28	166	88	256	82	121	07	211	04
5	25	10	1992	09	05	156	58	297	39	115	68	230	10
6	25	10	1992	12	26	134	62	285	31	74	69	213	16
7	25	10	1992	19	45	145	55	270	50	113	59	208	03
8	26	10	1992	06	45	168	76	261	81	125	16	34	04
9	30	10	1992	14	08	161	64	274	52	122	48	220	07
10	31	10	1992	01	43	150	62	264	53	113	50	209	05
11	04	11	1992	16	29	87	45	313	55	281	65	21	05
12	05	11	1992	18	41	161	66	254	83	120	22	25	12
13	05	11	1992	18	46	162	60	256	82	123	27	26	14
14	05	11	1992	19	16	164	57	259	82	127	30	27	17
15	06	11	1992	02	42	73	37	296	61	249	65	9	13
16	06	11	1992	04	11	168	54	269	75	135	36	34	14
17	07	11	1992	01	35	129	35	243	74	117	51	357	23
18	10	11	1992	11	17	163	49	263	78	132	37	27	19
19	10	11	1992	13	35	113	33	296	57	213	77	25	12
20	23	11	1992	22	58	124	62	243	47	85	54	220	08
21	02	12	1992	20	43	243	76	74	86	300	12	208	07
22	03	12	1992	06	38	172	74	267	72	130	24	220	01
23	22	01	1993	20	27	147	52	275	52	122	61	31	00
24	23	01	1993	00	04	74	57	326	65	287	44	22	05
25	17	02	1993	19	03	78	97	322	65	280	51	24	11
26	10	03	1993	19	26	113	59	274	33	50	74	196	13
27	04	05	1993	20	56	171	65	266	79	131	26	37	09
28	13	05	1993	08	38	132	66	263	35	81	61	204	17
29	13	06	1993	06	16	135	63	254	47	95	54	198	09
30	22	08	1993	17	58	75	56	304	46	288	62	188	05

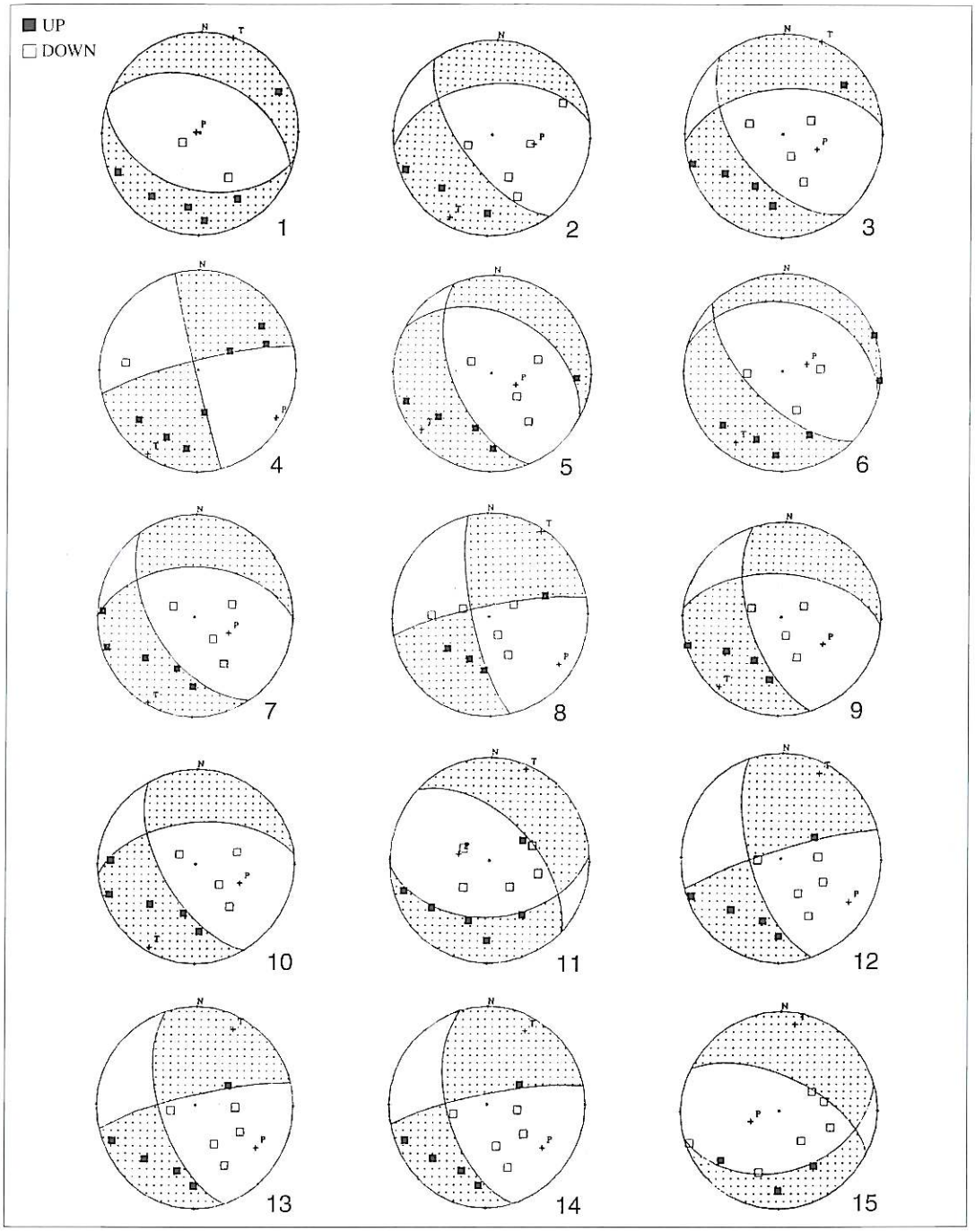

Fig. 7. Fault plane solutions of the thirty earthquake events studied. Focal mechanisms of the events are illustrated (*continued on p. 496*).

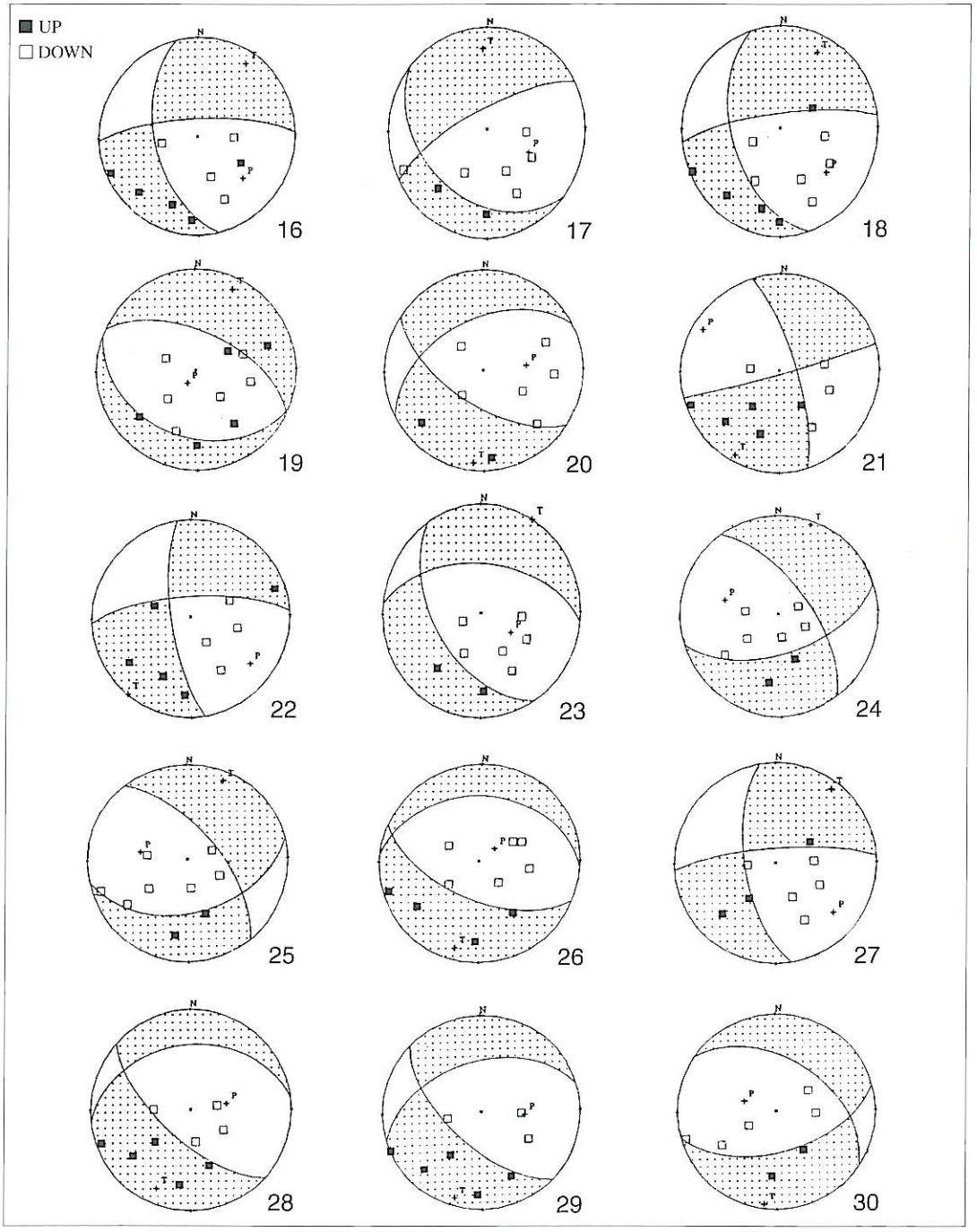

Fig. 7 *(continued).*

addition, the slip vector of group C is opposite to that of the other two groups. It clear that the events of group C took place on the edge of the aftershock zone. In general, it has been found (Savage and Meyer, 1985) that the reversal of the slip direction on the edge of aftershock zone is mainly due to a rebound mechanism, *i.e.* force pushing back on the moved segment of the fault. If the motion is nonuniform across the fault, a rebound could exist in some segments (Andrews, 1980). The orientation of the T axis deduced from the three composite solutions is approximately NNE-SSW. T axes have a maximum plunge of 17° and a mean value of about 9°. The low angle plunge indicates that the extensional mechanism is dominant in this region.

The fault plane solutions determined for the mainshock in the previous studies, based on the CMT harvard solution (Dziewonski *et al.*, 1993), teleseismic body wave inversion (E93; EL 98; H99) and the polarity data of the WWWSSN stations (A93; M93) are compared in fig. 8. Parameters of these solutions are listed in table VI. All of these solutions indicate a normal faulting mechanism with a component of right lateral strike slip motion on a fault plane trending E-W to ENE-WSW. The T axes of the fault planes reflect a NNE-SSW tensional stress. The focal depth obtained in the previous work (table VI) using the inversion technique of the first motion data (CMT; E93; EL98; H99) is almost the same (22, 23 km). The derived source time duration is 4 s (CMT; E93; H99). This result differs from EL98 which indicate a source duration of 3 s.

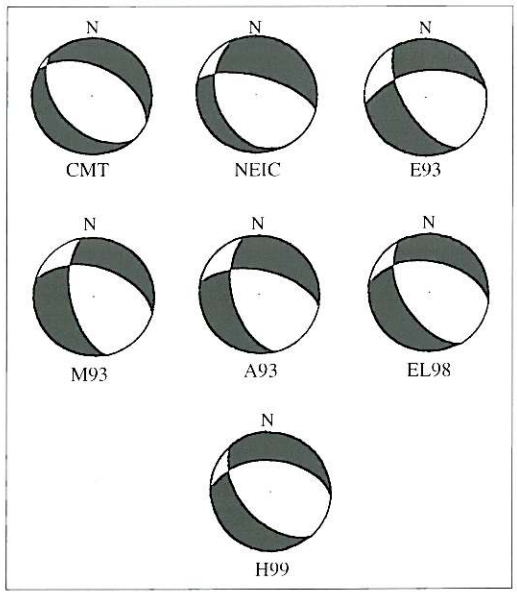

Fig. 8. Comparison of the fault plane solutions determined in different studies of the Cairo earthquake.

Comparison of the three composite solutions for the three groups of aftershocks with the mechanism of the mainshock indicates that groups A and B are similar to the mechanism

Table VI. Source models derived by different authors.

Reference	Strike deg.	Dip deg.	Rake deg.	Source duration s	Depth km
CMT	297	49.0	– 103.0	4	22
NEIC	285	66.0	– 117.0		
E93	262	54.0	– 144.0	4	23
M93	289	49.5	– 138.7		
A93	282	57.0	– 136.0		
EL98	280	47.5	– 128.0	3	23
H99	275	48.0	– 122.0	4	22

Notes: CMT = Harvard solution (Dziewonski *et al.*, 1993); NEIC = National Earthquake Information Center solution; E93 = El Hadidy (1993); M93 = Maamoun *et al.* (1993); A93 = Abou Elenean (1993); EL98: El-Sayed *et al.* (1998); H99 = Hussein (1999).

of the mainshock. The average slip direction is Az = 75° and plunge = 30°. The average T axis is Az = 37°, plunge = 8°. The slip direction of anomalous group C is also opposite to that of the mainshock. On the other hand, the composite solutions of the three groups and the mechanism of the mainshock are indicative of horizontal tension in the NNE-SSW direction.

5. Stress tensor analysis

The tectonic stress field due to the regional driving forces acting on a portion of the lithosphere is modified by the deformational processes that take place within the lithosphere. Thus, the observed tectonic stress field reflects not only the current dynamic stress conditions, but some of its characteristics are also inherited from conditions created by earlier tectonic evolution, in particular lateral heterogeneity and zones of weakness. The generation of an earthquake by brittle rupture at depth is a direct expression of the present stress field. The P and T axes are insufficient to represent this stress field (McKenzie, 1969). Gephart and Forsyth (1984) used the orientations of fault planes and slip directions indicated by a population of earthquake focal mechanisms to determine the best fit regional principal stress directions and as a measure of relative stress magnitudes R

$$R = \frac{(\sigma_2 - \sigma_1)}{(\sigma_3 - \sigma_1)}.$$

Where σ_1, σ_2 and σ_3 are the values of the maximum, intermediate and minimum compressive stress respectively. Three main assumptions are made: 1) stress is uniform in the rock volume investigated; 2) earthquakes are a shear dislocation on pre-existing faults, and 3) on each fault plane slip occurred in the direction of resolved shear stress. In order to define the discrepancies between the stress tensor and fault plane solutions, a misfit variable is introduced. The misfit of the solution is defined as the minimum rotation about any arbitrary axis that brings the fault geometry into an orientation that is consistent with the stress model. Searching through all orientations in space by grid technique operation in the whole space of stress parameters, the minimum sum of the misfit of all available fault plane solutions is obtained. The confidence limits of the best stress model are established by one-norm statistics (Gephart and Forsyth, 1984). Our database consists of 30 individual fault plane solutions (fig. 7 and table V). These solutions were used as input data for the stress tensor inversion. The inversion of these data yielded a misfit of 5.8. Stress inversion results for the earthquake set analyzed in this study are shown in table VII. The individual and overall best solutions for Dahshour area are explained in fig. 9. The stress field estimated by the stress tensor inversion method is extensional, with σ_3

Table VII. The stress tensor directions, stress ratio and degree of misfit using Gephart and Forsyth (1984) method.

σ_1		σ_2		σ_3		R	Misfit
Az.	Dip	Az.	Dip	Az.	Dip		
45	90	295	0	205	0	0.3	5.831 degree

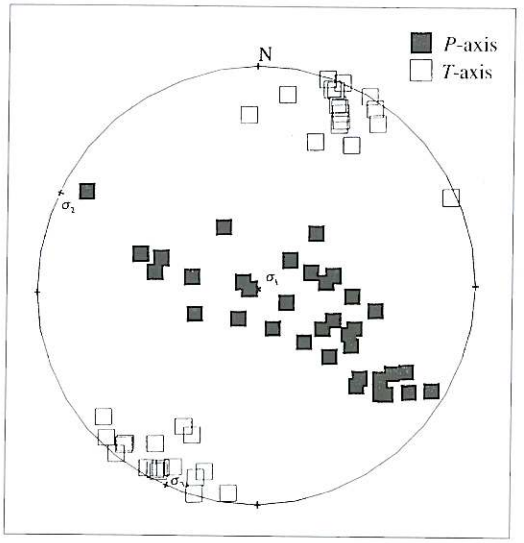

Fig. 9. The equal-area plot showing P and T axes deduced from the fault plane solutions and the preferred stress directions (σ_1, σ_2 and σ_3) of the stress tensor inversion.

in a direction of NNE-SSW and a near vertical σ_1. σ_3 axis has a plunge of 0° implying horizontal tensional stress. The nodal planes trending E-W to ENE-WSW conform to orientation of the stress tensor field estimated from inversion of the thirty mechanisms.

6. Spectral magnitudes

There are numerous quantitative measurements of the size of an earthquake, such as radiated energy, seismic moment or magnitude. Of these the most commonly used is the earthquake magnitude. Earthquake magnitudes are estimates of radiation intensities of a given wave type at a particular period. General agreement exists that body wave magnitude is insufficient to rate the strength of earthquakes on the basis of *P*-waves and that the radiation intensity of *S*-waves remains unknown due to its higher attenuation (Roslov, 1994). The body wave magnitudes published by NEIS are based on amplitude observations in the period range from 0.1 up to 3 s. Thus it is usually determined at periods shorter than the one of the maximum radiation, especially for larger earthquakes (Duda and Kaiser, 1989). Also body wave magnitudes, which are calculated from different instruments with different free periods of oscillation, usually yield different magnitude figures for a given earthquake. However, the broadband records of seismic waves enable one to extend the magnitude definition to bandpassed seismograms and to determine a set of magnitudes corresponding to the respective set of seismograms (Duda and Yanovskaya, 1994). The maximum spectral magnitude together with its period are considered diagnostic quantities for seismic events.

Duda and Yanovskaya (1994) found that it is better for determination of spectral magnitudes to use the spectrum instead of amplitudes from bandpass seismograms to avoid the effect of the band width. The magnitude spectrum $M_S(T)$ is obtained from the formula

$$M_S(T) = S_I(T) + \sigma_I(\Delta, h, T)$$

where I refers to either the vertical Z or radial R component of the ground velocity density $S_I(T)$ and $\sigma_I(\Delta, h, T)$ is the *P*-wave calibrating function. $M_S(T)$ is a distribution of magnitude values in the period range from $T_{min} = 2\Delta t$ (Δt is the sampling interval of the seismogram) to $T_{max} =$ = 60 s (length of the time window). Δ is the epicentral distance and h is the focal depth. The magnitude spectrum is subsequently averaged in period intervals of a width equal to one octave and centered at the periods 0.25, 0.5, 1, 2, 4, 8, 16 and 32 s. In this case the spectrum is smoothed and yields 8 discrete values. Figure 10 (curve B) shows the spectral magnitudes curves calculated for the main shock using the PASTA Program of Roslov (1994). The broadband stations used for spectral magnitudes are Col (Alaska, U.S.A.), KONO (Kongsberg, Norway) and MAJO (Matsushiro, Japan). Table VIII shows the average values of spectral magnitudes (M_S) over one octave period intervals of width and centered at the periods 0.25, 0.5, 1, 2, 4, 8, 16 and 32 s.

Kasier and Duda (1988) extracted the source parameters (seismic energy, seismic moment, fault length and stress drop), using the values of the maximum spectral magnitude through the magnitude spectrum curve and its corresponding period using the following equations:

$$M_0 = 10^{(mf)\max - 0.7} \cdot T_0 \cdot \left[2\rho(r)c(r)c(s)^4 / \pi R^2_{\theta\phi} \right]^{1/2} \quad (6.1)$$

$$T_0 = a / k \cdot c(s) \quad (6.2)$$

$$\Delta\sigma = \frac{7}{16} \frac{M_0}{a^3}, \text{ for circular fault model.} \quad (6.3)$$

Where M_0 is the seismic moment; (mf)max is the maximum value of the magnitude spectrum ((mf)max for the mainshock = 6.45); T_0 is the corner period corresponding to (mf)max ($T_0 =$ = 2.7 s); $\rho(r)$ is the density near the observation point (ρ = 2.7 g/cm^3); $c(r)$ and $c(s)$ are the velocities of the *P* wave near observation point and source region $c(r)$ = 6.1, $c(s)$ = 6.3 km/s; $R_{\theta\phi}$ is the radiation pattern factor for *P*-wave ($R_{\theta\phi}$ = 0.5 is used); a is the fault radius (fault length $L = 2a$); k is a constant depend on the specific source model under consideration and is

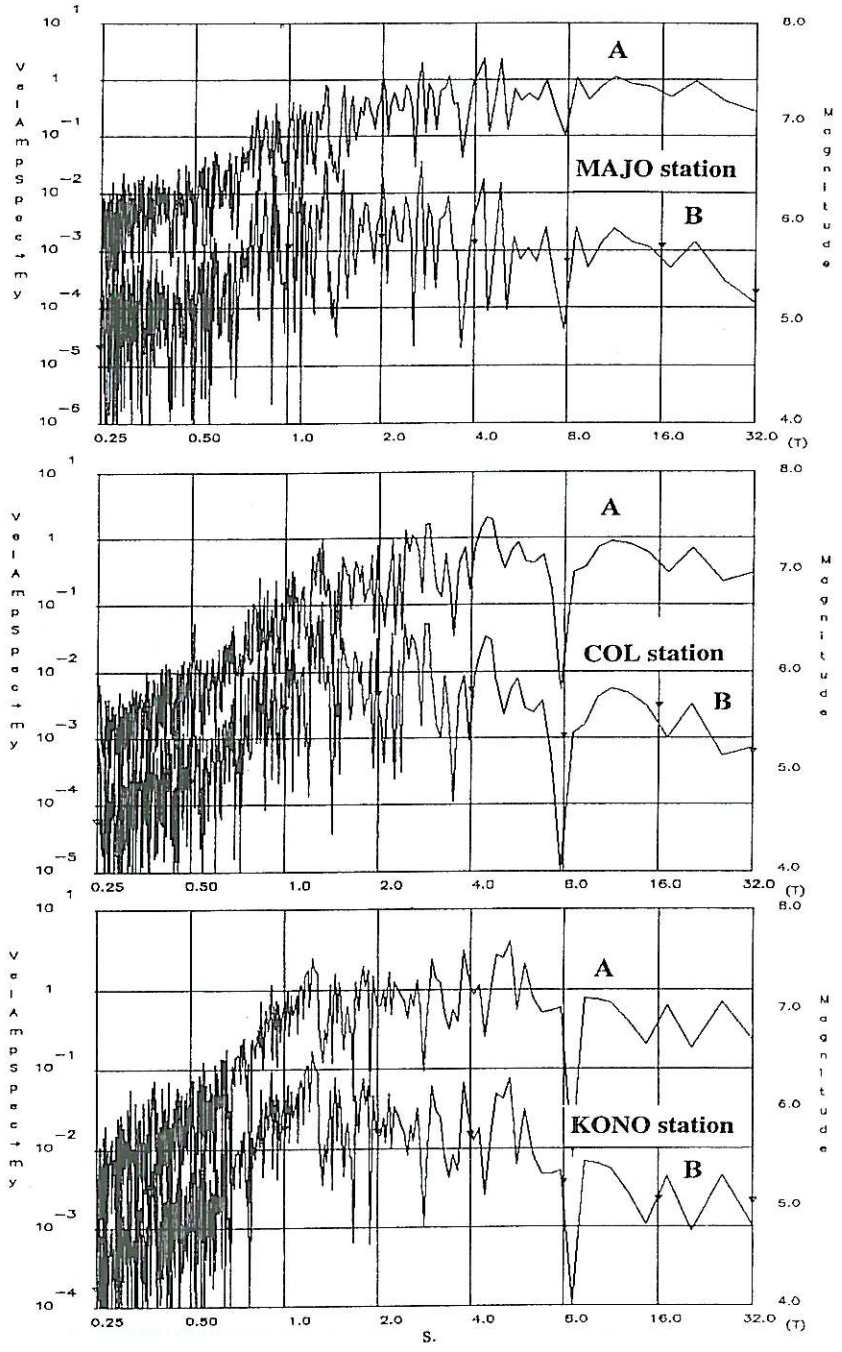

Fig. 10. Magnitude spectrum and velocity spectrum. Curve A represents the velocity spectra while B represents magnitude spectra.

Table VIII. Average values of the spectral magnitudes.

Period	0.25	0.5	1.0	2.0	4.0	8.0	16.0	32.0
M_s	4.74	4.92	5.72	5.77	5.78	5.41	5.5	5.18

Table IX. Source parameters of the 1992 Cairo earthquake estimated by different authors.

Reference	Maamoun *et al.* (1993)	Al Ibiary (1993)	El Hadidy (1993)	NEIC	HRVD Dziewonski *et al.* (1993)	El Sayed 1998	Hussein (1999)	This study spectral magnitude
Moment (Nm)	8.0E17	9.1E17	6.99E17	5.0E17	5.6E17	5.2E17	7.2E17	9.97E17
Stress drop (MPa)	0.70	0.648	2.30				1.85	0.76
Radius (km)	7.5	8.5	4.5				5.5	6.9
Area (km^2)	110	227	81.0				99.0	149.49
Dislocation (m)	0.13	0.13	0.22				0.245	0.22

a function of azimuth ($k = 0.37$); $\Delta\sigma$ is the stress drop obtained by Keilis-Borok (1959) equation.

The average displacement (Aki, 1966) along the fault can be calculated by the formula

$$U = M_0/\mu S \qquad (6.4)$$

where μ is the shear modulus; S is the fault area (πa^2).

Table IX shows the calculated source parameters following the above procedure. The source parameters calculated in the previous works are also listed in the same table.

The seismic moment calculated using the spectral analysis technique (Al Ibiary, 1993), HRVD moment tensor solution (Dziewonski *et al.*, 1993), NEIC moment tensor solution and body wave inversion technique (El Hadidy, 1993; El Sayed *et al.*, 1998 ; Hussein, 1999) and the preliminary reported value of the moment by HRVD (Maamoun *et al.*, 1993) ranges from 5.0E17 to 9.1E17 n-m. These integral values are not grossly different from our results. Fault radius estimated from the spectral corner frequency (Al Ibiary, 1993), from the corner period corresponding to the maximum value of the magnitude spectrum (this study) and from the aftershock distribution (Maamoun *et al.*, 1993) is somewhat larger than the 4.5-5.5 km values estimated using the body wave inversion technique (El Hadidy, 1993; Hussein, 1999).

Considering the different methods used in the calculation of the source parameters, the source parameters estimated previously and in this study are not exactly the same. It is well known that the stress drop and displacement require the estimation of the rupture area from the aftershocks (El Hadidy, 1993; Maamoun *et al.*, 1993; Hussein, 1999) or from the spectral corner frequency (Al Ibiary, 1993) or from the corner period corresponding to the maximum value of magnitude spectrum (this study). The rupture area estimated using the different methods will not be similar. Therefore, the estimated values of the stress drops will vary.

7. Discussion and conclusions

The $M_w = 5.8$ earthquake of 12th October, 1992 is the largest instrumentally recorded earthquake in Dahshour region. The spectral magnitude calculations of three broadband stations, using the technique of Duda and Yanovskay (1994) give a maximum average spectral magnitude of about 5.78 corresponding to a period of four seconds. The calculation of spectral magnitudes from the broadband stations at different epicentral distances and azimuths yields a stable estimate of the radiation intensity of *P*-wave *i.e.* magnitude. All the previous studies are in agreement with regard to the depth of this earth-

quake (22-23 km). Although this earthquake is classified to be small event (magnitude less than 6.0), it produced significant injuries, loss of life and damage to property. Significant damage was found mostly in adobe or non-reinforced masonry buildings and non-engineered reinforced concrete buildings (Japanese Expert Team, 1993). Although the soft soil cover in El Aiyat and El Faiyum amplified the acceleration two-times (El Sayed *et al.*, 1998), the estimated acceleration of about 0.5 m s^{-2} cannot alone explain the relatively large numbers of damaged structures. The damage was noted mostly in the buildings that were illegally constructed or constructed by poor construction work. The October, 1992 Cairo earthquake is the first disastrous event to have occurred in this region since the 1847 event after a lapse of 145 years. In our case, where there is no recent recorded seismicity in this region, detailed seismological investigations of the mainshock and aftershocks during the 1992 earthquake offer the only means for understanding the present tectonics and source characteristics in this region.

Fault plane solutions of the mainshock obtained by different authors are compatible with E-W to ENE-WSW striking normal fault with a dextral strike slip motion. The subsidence of the left-hand side of the asphalt road between Aiyat and Giza supports the occurrence of a normal faulting mechanism.

The three composite fault plane solutions (A, B and C) obtained from the analysis of the *P* wave polarity data for thirty aftershocks demonstrate mainly E-W to ENE-WSW trending dip slip fault planes with right lateral strike slip component. The present fault plane solutions correlate well with the dominant E-W fault trend in this region. *T* axes of the fault planes obtained from the mainshock and the three composite solutions are oriented in a NNE-SSW direction and are nearly horizontal. This extensional regime is the main cause of the dip slip motion with a strike slip component. The composite focal mechanism solution obtained for the first two groups (A and B) is almost consistent with the mainshock fault plane solution. Furthermore, the slip vector direction for them is also consistent. On the other hand, the slip direction for the composite solution of group C events that took place on the edge of the aftershock zone is opposite to that of the mainshock and the other two groups. This may be due to a rebound mechanism near the edge of the aftershock zone.

Epicenters of the well-located aftershocks were not distributed along the E-W trend but instead occurred as a cluster of seismicity. Savage and Meyer (1985) interpreted the clustering as being due to increased stress following the mainshock, which may have had most of its movement in a linear feature. Most of the aftershocks following the Cairo earthquake took place below the mainshock fault plane. This mechanism would suggest that the aftershock activity resulted from subsidiary faulting in the adjacent fault blocks along the surface subparallel to the primary fault (Mendoza and Hartzell, 1988). Although the aftershocks do not fall on a simple fault plane in the cross section, the mechanism of groups A and B were almost similar and similar to the mechanism of the mainshock. These two groups include the polarity data for 22 aftershocks, representing 73% of the events used for constructing the three composite solutions A, B and C. This means that the majority of aftershock movement took place in the same sense as the mainshock. Several studies (*e.g.*, Deschamps and King, 1984) have reported a similar behavior in well-studied recent earthquakes, suggesting a simple stress description. In our case, it can be seen that the three groups of aftershocks have almost the same *T* axes as the mainshock.

The tectonic stress orientation estimated by the inversion of the fault plane solutions of the thirty earthquakes using the method of Gephart and Forsyth (1984), is in good agreement with the stress regime derived from the three composite solutions with a tensile axis (σ_3) trending to NNE-SSW while the compressional axis (σ_1) trend in a NW-SE direction. The tensional axis (σ_3) is horizontal while the compressional axis ($\sigma 1$) is vertical. This stress model is more consistent with the nodal planes trending E-W and ENE-WSW.

The stress orientation indicated by composite solutions is in agreement with the stress field results obtained by the inversion of the individual events. This stress field represents the present day stress field. The fault planes determined correlate well with the faulting in this area.

Therefore, it is concluded that the area of study is characterized by extensional stress regime oriented in a NNE-SSW direction. The extensional stress is the main source of dip slip faults with strike slip component in the region of study. According to Pondrelli *et al.* (1995), the northeastern corner of Africa, including the northern part of Egypt is subjected to tensional stress. This stress field may be related to the counterclockwise rotation of Africa with respect to Eurasia that produces northwestern convergence along the boundary. The direction of extension has been estimated as ENE-WSW (Meshref, 1990). This direction of extension agrees well enough with the stress pattern in the Northern Red Sea rift zone. The area of the present study is located between the compressional tectonics of the Eastern Mediterranean Sea and the extensional zone of the Northern Red Sea rift zone (fig. 11). Thus, taking into consideration this complex compressional- tensional geometry the tensional stress axis changes its direction to NNE-SSW in the area of study.

For the mainshock, the dynamic source parameters were calculated using spectral magnitude techniques. The seismic moment calculated in this work and previous studies for this event ranges from 5.0E17 to 9.97E17 n-m. The stress drop $\Delta\sigma$ estimated in this study is nearly consistent with the previously calculated values, in which the rupture area was estimated from the aftershocks or from the spectral corner frequency ($\Delta\sigma$ = 0.65-0.76 MPa). These values are somewhat lower than the 1.85-2.3 MPa stress drop estimated from the rise time using the body wave inversion technique.

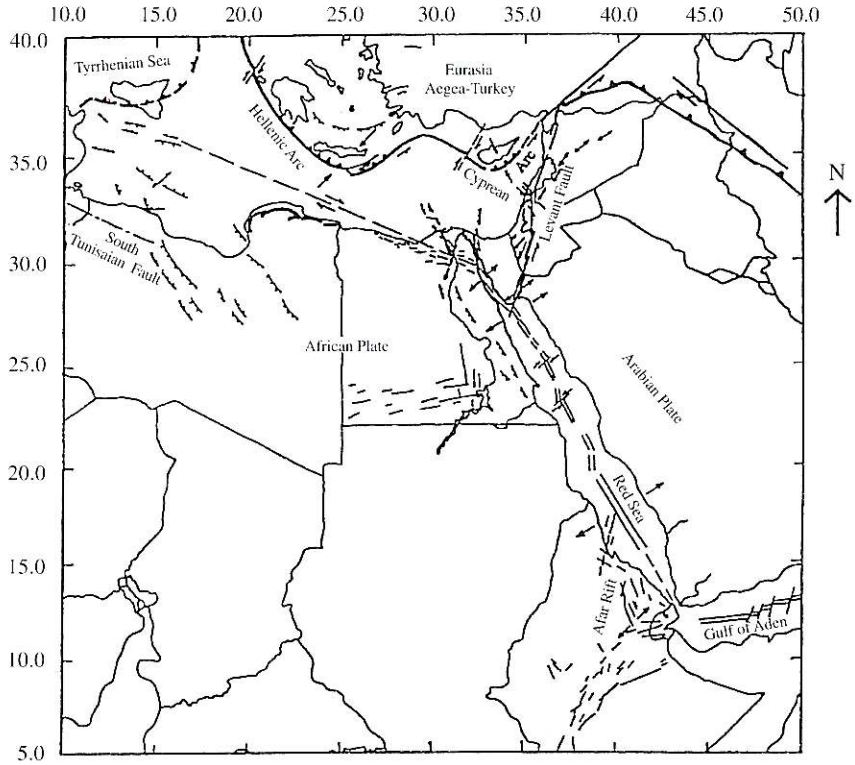

Fig. 11. Regional tectonic map of Egypt (after Abou Elenean, 1993) reflecting the direction of the tectonic stresses in the study area and the surrounding regions.

REFERENCES

ABD EL-TAWB, S., A.M. HELAL, H. DEWEIDAR and A. EL-SAYED (1993): Surface tectonic features of 12 October 1992 earthquake, Egypt, at the epicentral area, *Ain Shams Sci. Bull.*, special issue, 124-136.

ABOU ELENEAN, K. (1993): Seismotectonics of the Mediterranean region north of Egypt and Libya; *M.Sc. Thesis*, Faculty of Science, Mansoura University, Egypt.

AKI, K. (1966): Generation and propagation of *G* waves from the Niigata earthquake at June 16, 1964, *Bull. Earthquake. Res. Inst.*, Tokyo Univ., **44**, 73-88.

AL IBIARY, M. (1993): Geophysical contribution on October 12th, 1992 earthquake Ain Shames Geophysical Research Team, *Ain Shames Univ. Report*, Cairo, Egypt.

ANDREWS, D.J. (1980): A stochastic fault model, 1: static case, *J. Geophys. Res.*, **85**, 3867-3877.

DESCHAMPS, A. and G.C.P. KING (1984): Aftershocks of the Campania-Lucania earthquake of 23 November, 1980, *Bull. Seismol. Soc. Am.*, **74** (6), 2483-2517.

DUDA, S. and D. KAISER (1989): Spectral magnitudes, magnitudes spectra and earthquake quantification; the stability issue of the corner period and of the maximum magnitude for a given earthquake, *Tectonophysics*, **166**, 205-219.

DUDA, S. and T. YANOVSKAYA (1994): Calibrating functions for *P*-wave spectral magnitudes, *Acta Geophys. Pol.*, **42** (4), 293-306.

DZIEWONSKI, A.M., G. EKSTRÖM and M.P. SALGNIK (1993): Centriod moment tensor solution for October-December, 1992, *Phys. Earth Planet. Inter.*, **80**, 89-103.

EL HADIDY, S. (1993): Source process of the 1992 Cairo, Egypt earthquake using far field seismogram, *Report for the Course of Seismolgy 1992-1993*, IISEE, Japan.

EL HADIDY, S. (1995): Crustal structure and its related causative tectonics in Northern Egypt using geophysical data, *Ph.D. Thesis*, Ain Shams University, Cairo, Egypt.

EL SAYED, A., R. ARVIDSSON and O. KULHANCK (1998): A case study of small destructive event, *J. Seismol.*, **2**, 293-302.

GEPHART, J. and W. FORSYTH (1984): An improved method of determining the regional stress tensor using earthquake focal mechanism data: application to the San Fernando earthquake sequence, *J. Geophys. Res.*, **89** (B11), 9305- 9320.

HUSSEIN, H.M. (1999): Source process of the October 12, 1992 earthquake, *Ann. Geofis.*, **42** (4), 665-674.

JAPANESE EXPERT TEAM (1993): Report of Japan Disaster Relief Team on the earthquake in Arab Republic of Egypt of October 12, 1992.

KAISER, D. and S. DUDA (1988): Magnitude spectra and other source parameters for some major 1985 and 1986 earthquakes, *Tectonophysics*, **152**, 303-318.

KEBEASY, R., M. MAAMOUN and R. ALBERT (1981): Earthquake activity and earthquake risk around Alexandria area in Egypt, *Acta Geophys. Pol.*, **29** (1), 1-18.

KEILIS-BOROK, V. (1959): On estimation of the displacement in an earthquake source dimension, *Ann. Geofis.*, **12**, 205.

LEE, W. and S. LAHR (1972): HYPO71, a computer program for determining hypocenter, magnitude and first motion of local earthquakes, *U.S. Geol. Surv., Open-File Rep.*

MAAMOUN, M.E., A. MEGHAED, A. HUSSIN and I. MARZOUK (1993): *Preliminary Studies on Dahshour Earthquake*, National Research Institute of Astronomy and Geophysics, Cairo, Egypt (abstract).

MARZOUK, I. (1987): Crustal structure studies in Egypt, *Ph.D. Thesis*, Hamburg University, Germany.

MCKENZIE, D. (1969): The relation between fault plane solutions of earthquakes and direction of the principal stresses, *Bull. Seismol. Soc. Am.*, **59**, 591-601.

MENDOZA, C. and S.H. HARTZELL (1988): Aftershock patterns and mainshock faulting, *Bull. Seismol. Soc. Am.*, **78** (4), 1438-1449.

MESHREF, W. (1990): Tectonic framework, in *The Geology of Egypt*, edited by R. SAID (A.A. Balkema, Rotterdam, Netherlands), 113-155.

PONDRELLI, S., A. MORELLI and E. BOSCHI (1995): Seismic deformation in the Eastern Mediterranean area estimated by moment tensor summation, *Geophys. J. Int.*, **122** (3), 938-952.

REFAI, E., S. RIAD and A. TEALEB (1973): The main tectonic trends of west Cairo area, *HIAG Bull.*, No. 102.

ROBERSTON RESEARCH INTERNATIONAL (BRI) and ASSOCIATED RESEARCH CONSULTANTS IN ASSOCIATION WITH SCOTT PICKFORD and ASSOCIATES LIMITED and ERC ENERGY RESOURCE CONSULTANTS LIMITED (1982): Petroleum Potential evaluation, Western Desert, ARE, *Report prepared for EGPC*, vol. 8.

ROSLOV, Y. (1994): Program for amplitude spectrum treatment and analysis, *Acta Geophys. Pol.*, **42** (4), 315-319.

SAVAGE, M.K. and R.P. MEYER (1985): Aftershocks of an $M = 4.2$ earthquake in Hawaii and comparison with long term studies of the same volume, *Bull. Seismol. Soc. Am.*, **75** (3), 759-777.

SEHIM, A., A. ISMAIL and R. MAHMOUD (1992): Proposed structural model, Khalada West Concession, Western Desert, Egypt, *EGPC Eleventh Exploration and Production Conference, November1992, Cairo*, 79-97.

SOUFLERIS, C., J.A. JACKSON, G.C.P. KING, C.P. SPENCER and C.H. SHOLZ (1982): The 1987 earthquake sequence near Thessaloniki (Northern Greece), *Geophys. J. R. Astron. Soc.*, **68**, 429-458.

SUETSUGU, D. (1995): *Earthquake Source Mechanism*, IISEE, Building Research Institute, Japan.

THE EGYPTIAN GEOLOGICAL SURVEY and MINING AUTHORITY (1981): *Geological Map of Egypt*, 1:2000000.

THE EGYPTIAN GEOLOGICAL SURVEY and MINING AUTHORITY (1993): *A Preliminary Report on the Dahshour Earthquake, 12th October, 1992.*

(received July 24, 1999;
accepted March 2, 2000)